

Creating Artificial Ice States Using Vortices in Nanostructured Superconductors

A. Libál, C.J. Olson Reichhardt, and C. Reichhardt

Theoretical Division, Los Alamos National Laboratory, Los Alamos, New Mexico 87545

(Dated: May 15, 2009)

We demonstrate that it is possible to realize vortex ice states that are analogous to square and kagomé ice. With numerical simulations, we show that the system can be brought into a state that obeys either global or local ice rules by applying an external current according to an annealing protocol. We explore the breakdown of the ice rules due to disorder in the nanostructure array and show that in square ice, topological defects appear along grain boundaries, while in kagomé ice, individual defects appear. We argue that the vortex system offers significant advantages over other artificial ice systems.

PACS numbers: 74.25.Qt

Geometric frustration occurs when a system is constrained by geometry in such a way that the pairwise interaction energy cannot be simultaneously minimized for all constituents, and appears in water ice [1], spin systems [2, 3, 4], and a variety of other systems in both physics [5] and biology [6]. A specific example of frustration occurs in the classical spin ice system where the constituents of the system are magnetic spins on a grid of corner-sharing tetrahedra. The spins are constrained to point along the lines connecting the middle points of the tetrahedra [3, 4] and pairs of spins can minimize their energy by adopting a head-to-tail configuration. It is not, however, possible for the four spins on a tetrahedron to simultaneously satisfy each of the six pairwise interactions in a head-to-tail fashion; the best the system can do is to satisfy four interactions out of six, leaving two pairs in a head-to-head or tail-to-tail configuration. As a result, in the ground state configuration each tetrahedron obeys the so-called ‘‘ice rule’’ of a two-in two-out configuration with two spins pointing toward the center of the tetrahedron and two spins pointing away from it. Defects appear in the form of magnetic monopoles [7].

Recently, there has been growing interest in creating model systems that exhibit spin ice behavior [8, 9, 10, 11, 12, 13, 14] and that allow the individual constituents to be imaged directly, unlike molecular or atomic ices. For example, Wang *et al.* [8] created artificial square ice using single-domain rectangular ferromagnetic islands arranged in a square lattice such that four islands meet at every vertex point. They found that as the inter-island interaction increased, the system preferentially formed ice-rule-obeying vertices, but it did not reproduce the known ground state of two-dimensional (2D) spin ice, where the two ‘‘in’’ magnetic moments are on opposite sides of the vertex. This could be due to the relative weakness of the magnetic interactions. It has recently been shown that certain dynamical annealing protocols permit the system to approach the ground state more closely [9, 10]. Similar studies have been performed for a 2D kagomé ice system [12, 13] where the local ice-rules were obeyed and defects such as three-in or three-out were absent [13]. In the colloidal artificial ice system of Ref. [14], the local dynamics can be accessed easily via

video microscopy; however, the ice arrays in this system are limited to relatively small sizes in experiment.

Here we propose that a particularly promising artificial ice system could be created using vortices in superconductors with appropriately designed nanostructured arrays of artificial pinning sites. There has been extensive experimental work showing that a rich variety of different pinning array geometries can be fabricated [15, 16, 17, 18, 19, 20], and various types of experimental techniques exist for directly imaging vortices in these arrays [17, 18, 19, 21]. The vortex system has several advantages over other artificial ice systems. The vortex-vortex interaction strength is large, permitting the ground state to be reached much more readily than in the nanomagnetic systems. An applied external current permits the straightforward realization of different dynamical annealing protocols. New types of defects can be studied by merely increasing or decreasing the magnetic field to create vacancies or interstitials that locally break the ice rules, while transport properties and critical currents can be measured which are not accessible in the other systems.

To form square vortex ice, we propose using an arrangement of elongated double-well pinning sites. Non-superconducting islands with the double-hump shape illustrated in Fig. 1(a) placed within a superconducting layer have a pair of potential minima at the highest points of the island where the superconducting layer is the shallowest. A single vortex trapped over each island will sit at one of the two minima, depending on the interactions with nearby vortices. By changing the arrangement of the islands, different types of ice can be created. For square ice, shown in Fig. 1(a), four islands come together at each vertex and the state of each island is defined as ‘‘in’’ if the vortex sits close to the vertex and ‘‘out’’ otherwise. We define n_{in} as the number of ‘‘in’’ vortices at a vertex. In Fig. 1(a), the vortices have formed an $n_{in} = 2$ ice-rule-obeying ground state configuration. Figure 1(b) shows a kagomé spin ice arrangement with three islands surrounding each vertex. In this case, the lowest energy state has $n_{in} = 1$ or $n_{in} = 2$ at each vertex, but there is no overall ordering into a unique ground state.

To study the vortex ice, we perform numerical simula-

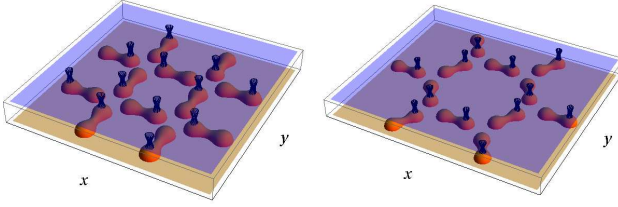


FIG. 1: Schematic of the nanostructured pinning site configurations producing ice states. Double-lobed objects: pins; open mesh objects: vortices. a) Square ice ground state. b) One possible biased ground state of the kagomé ice system.

tions of a 2D sample with periodic boundaries containing N_p elongated pinning sites in the square or kagomé configurations illustrated in Fig. 1 and $N_v = N_p$ vortices. A vortex i at position \mathbf{R}_i obeys the following overdamped equation of motion: $\eta(d\mathbf{R}_i/dt) = \mathbf{f}_i^{vv} + \mathbf{f}_i^s + \mathbf{f}^d + \mathbf{f}_i^T$. The damping constant $\eta = \phi_0^2 d / 2\pi\xi^2 \rho_N$, where $\phi_0 = h/2e$ is the flux quantum, ξ is the superconducting coherence length, ρ_N is the normal state resistivity of the material, and d is the thickness of the superconducting crystal. The vortex-vortex interaction force is given by $\mathbf{f}_i^{vv} = \sum_{j \neq i}^{N_v} f_0 K_1(R_{ij}/\lambda) \hat{\mathbf{R}}_{ij}$, where K_1 is the modified Bessel function appropriate for stiff three-dimensional vortex lines, λ is the London penetration depth, $f_0 = \phi_0^2 / (2\pi\mu_0\lambda^3)$, $R_{ij} = |\mathbf{R}_i - \mathbf{R}_j|$, and $\hat{\mathbf{R}}_{ij} = (\mathbf{R}_i - \mathbf{R}_j)/R_{ij}$. The substrate force \mathbf{f}_i^s arises from the elongated pins, $\mathbf{f}_i^s = \sum_k^{N_p} f_0 (f_p/r_p) R_{ik}^{\pm} \Theta(r_p - R_{ik}^{\pm}) \hat{\mathbf{R}}_{ik}^{\pm} + f_0 (f_p/r_p) R_{ik}^{\perp} \Theta(r_p - R_{ik}^{\perp}) \hat{\mathbf{R}}_{ik}^{\perp} + f_0 (f_b/l) (1 - R_{ik}^{\parallel}) \Theta(l - R_{ik}^{\parallel}) \hat{\mathbf{R}}_{ik}^{\parallel}$. Here $R_{ik}^{\pm} = |\mathbf{R}_i - \mathbf{R}_k^p \pm l \hat{\mathbf{p}}_{\perp}^k|$, $R_{ik}^{\perp, \parallel} = |(\mathbf{R}_i - \mathbf{R}_k^p) \cdot \hat{\mathbf{p}}_{\perp, \parallel}^k|$, \mathbf{R}_k^p is the position of pin k , and $\hat{\mathbf{p}}_{\parallel}^k$ ($\hat{\mathbf{p}}_{\perp}^k$) is a unit vector parallel (perpendicular) to the axis of pin k . Each vortex is constrained to stay within a pin composed of two half-parabolic wells of radius $r_p = 0.4\lambda$ separated by an elongated region of length $2l$ which confines the vortex perpendicular to the pin axis and has a repulsive potential or barrier of strength f_b parallel to the axis which pushes the vortex out of the middle of the pin into one of the ends. We take $l = 2/3\lambda$ or $5/6\lambda$ and vary the lattice constant a of the pinning array between $a = 2.0\lambda$ and 8.0λ . The driving force \mathbf{f}_d represents the Lorentz force from an applied current. The thermal force \mathbf{f}_i^T comes from thermal Langevin kicks and is set to zero except during the annealing of the kagomé ice.

Square Ice - We prepare the square ice system using a dynamical annealing procedure inspired by the nano-magnetic ice results of Refs. [9, 10]. In our simulations, we place one vortex in each pin at a random position and then use a protocol of a rotating in-plane applied current with decreasing amplitude, $\mathbf{f}^d = A_{ac}(t)(\cos(2\pi t/T_r)\hat{\mathbf{x}} + \sin(2\pi t/T_r)\hat{\mathbf{y}})$, where $T_r = 1000$ simulation time steps, $A_{ac}(t) = \pm(A_0 - \delta A[t/\delta t])$, $A_0 = 2.0f_0$, $\delta t = 10000$ simulation time steps, and $\delta A = 0.01f_0$. The force direction is reversed each time the magnitude of the force is de-

creased. We measure the number of vertices of each type that appear after completing the dynamical annealing. For the kagomé ice system, we obtain the vortex configurations from standard thermal simulated annealing.

To determine how effectively the dynamical annealing protocol brings the square ice system to the ground state, we introduce disorder to the system by replacing the delta-function distributed barriers f_b at the center of each pinning site with barriers of normally distributed strength, where the mean strength is f_b and the width of the distribution is σ . In Fig. 2 we illustrate the vertices that have reached the ground state configuration of $n_{in} = 2$ in a square ice sample with $a = 2.5\lambda$, $l = 5/6\lambda$ and $f_b = 0.25f_0$ for differing disorder widths σ . The dots represent vertices in the ice-rule obeying ground state, while the closed black circles indicate higher energy vertices that we term ice-rule defects D_I since they still obey the $n_{in} = 2$ ice rule but have the two “in” vortices adjacent to one another. The open circles mark the highest energy vertices that we term non-ice-rule defects D_{NI} since they do not obey the $n_{in} = 2$ ice rule but have, for example, $n_{in} = 3$ or $n_{in} = 0$. For $\sigma < 0.1$, the system can reach the ordered ground state as shown in Fig. 2(a). As the central barriers of the pins become more nonuniform with increasing σ , some pinning centers act as nucleation sites for grain boundaries, as illustrated in Figs. 2(b,c) for $\sigma = 0.1$ and $\sigma = 0.5$. In general, we find that for $0.1 < \sigma < 0.7$, all of the defected vertices form closed loop grain boundaries and the ratio of D_I to D_{NI} is 1:1 due to geometric constraints. For $\sigma \geq 0.7$, Fig. 2(d) shows that a proliferation of D_{NI} occurs so that the D_{NI} outnumber the D_I . The grain boundary loops interact and wind around the sample, making it difficult to determine the relation between σ and the grain boundary length. We find that individual D_{NI} can appear outside of grain boundaries, while D_I always remain confined to grain boundaries, suggesting that there could be a disorder-induced phase transition when the D_{NI} proliferate. We also find that doubly occupied pinning sites with two vortices each can act as grain boundary nucleation sites, as illustrated in the inset of Fig. 4(b).

In Figure 3(a), we plot the percentage of vertices P_{GS} that are in the ice-rule obeying ground state as a function of time during the dynamical annealing procedure in a sample with $a = 2.5\lambda$, $l = 5/6\lambda$, $f_b = 0.25f_0$, and different values of σ . At early times, when $|A_{ac}|$ is close to A_0 , all of the vortices follow the drive and switch back and forth inside the pinning sites. As $|A_{ac}|$ decreases, a transition occurs when the vortices cease to follow the driving direction and become locked into one position in the pinning site. For $\sigma = 0$, this locking transition is relatively sharp and occurs at $|A_{ac}| \approx 0.82f_0$. Nonzero values of σ broaden the transition significantly and cause some vertices to lock into the ground state at much earlier times; at the same time, complete locking of all vertices into the ground state can no longer be achieved within the finite time of the dynamical annealing process. We quantify the broadening of the transition

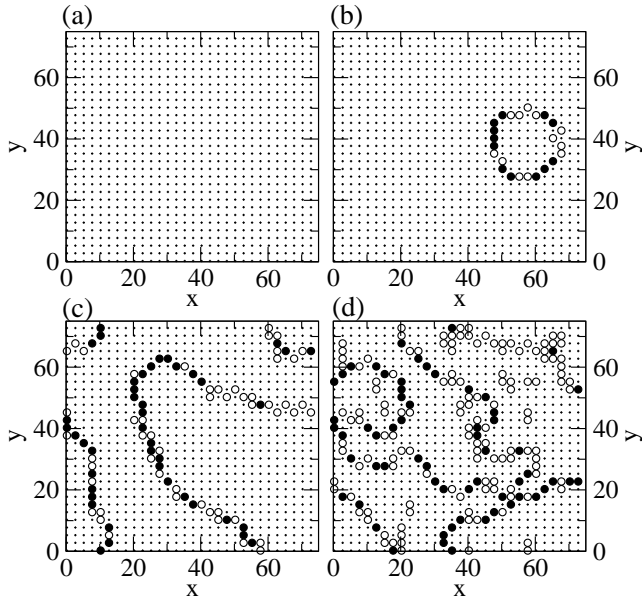


FIG. 2: Grain boundary images in square ice samples with $a = 2.5\lambda$, $l = 5/6\lambda$, and $f_b = 0.25$ for increasing disorder width σ . Dots: ground state $n_{\text{in}} = 2$ ice-rule obeying vertices; filled black circles: ice-rule defects D_I ; white circles: non-ice-rule defects D_{NI} . (a) $\sigma = 0$. (b) $\sigma = 0.1$. (c) $\sigma = 0.5$. (d) $\sigma = 1.0$.

with increasing σ by fitting the curves in Fig. 3(a) to the form $P_{GS}(t) = 1 - \exp(t/\tau)$. Figure 3(b) shows the fitted relaxation time τ as a function of σ and indicates the occurrence of an increasingly slow locking process as the disorder width increases. The dependence of P_{GS} on both a and σ is summarized in Fig. 3(d) for a system with $f_b = 1.0$ and $l = 2/3\lambda$. Here, P_{GS} decreases both with increasing σ and with increasing a as the relative strength of the vortex-vortex interactions decreases.

Depending on the system parameters, it is not always necessary to perform a dynamical annealing procedure in order to reach the ground state. To demonstrate this, we prepare the sample in a random state and then apply a fixed amplitude rotating drive, $\mathbf{f}^d = \tilde{A}(\cos(2\pi t/T_r)\hat{\mathbf{x}} + \sin(2\pi t/T_r)\hat{\mathbf{y}})$, with $\tilde{A} = 0.01f_0$ and $T_r = 1000$ simulation time steps, for 2×10^6 simulation time steps. When the central barrier in the pin f_b is weak, the system can reach the ordered ground state under the weak external shaking. For larger f_b , the system cannot reach the ordered ground state without dynamical annealing. This is shown in Fig. 3(c), where we plot the final P_{GS} at the end of the simulation time versus f_b for samples with $\sigma = 0.01$ and varied pinning lattice constant $a = 2.0\lambda$, 2.5λ , and 3.0λ . For large f_b , the sample is immediately frozen into the disordered initial configuration, and $P_{GS} \approx 0.125$, consistent with the value expected in a completely random sample. As f_b is lowered, a spontaneous rearrangement into a partially ordered state becomes possible and $P_{GS} > 0.125$. The value of f_b at which the spontaneous ordering appears increases with

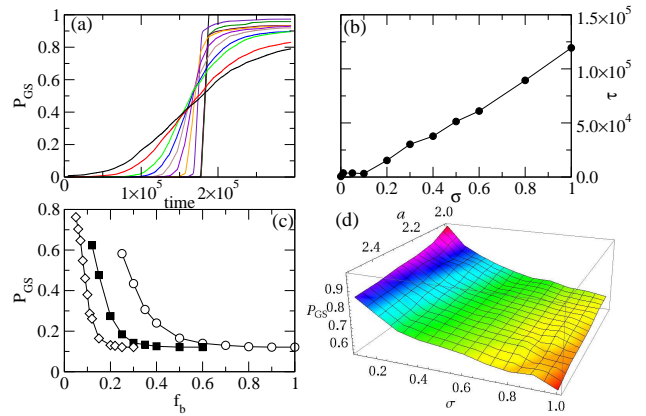


FIG. 3: (a) Percentage P_{GS} of ice-rule obeying ground state vertices vs time during the dynamical annealing process for different disorder widths σ . From upper right to lower right, $\sigma = 0, 0.01, 0.05, 0.1, 0.2, 0.3, 0.4, 0.5, 0.6, 0.8$, and 1.0 . Here, $a = 2.5\lambda$, $l = 5/6\lambda$, and $f_b = 0.25$. (b) Relaxation time τ vs σ for the same system. (c) Final value of P_{GS} vs f_b in samples subjected to a small shaking field with no dynamical annealing. Here $l = 5/6\lambda$, $\sigma = 0.1$, and $a = 2.0\lambda$ (open circles), 2.5λ (filled squares), and 3.0λ (open diamonds). (d) P_{GS} vs σ and a in a sample with $f_b = 1.0$ and $l = 2/3\lambda$.

decreasing a , indicating that as the vortex-vortex interactions grow stronger in the denser pinning arrays, the ordered ground state is much more energetically favored.

Kagomé ice - The kagomé lattice illustrated in Fig. 1(b) has a distinct set of ice rules from the square lattice. High energy vertices with $n_{\text{in}} = 0$ or 3 are avoided in favor of the kagomé-ice-rule obeying vertices with $n_{\text{in}} = 1$ or 2 . This system can form a non-unique ordered ground state, but only in the presence of an external biasing field. In Fig. 4(a) we show one possible biased ordered ground state for a kagomé lattice with $f_b = 1.0$ and $\sigma = 0$ obtained by applying a constant drive $\mathbf{f}^d = 0.01f_0(\hat{\mathbf{x}} + \hat{\mathbf{y}})$ along a lattice symmetry direction while performing simulated annealing. In the absence of the biasing force, some high energy defect vertices which take the form of monopoles appear in the system and there is no overall order, as illustrated in Fig. 4(c). We find that the kagomé ice is more robust against the effects of disorder than the square ice, in agreement with experimental findings for nanomagnetic kagomé ice [13]. The defect patterns are distinct from the square ice since no grain boundary state forms for the kagomé ice due to the lack of an ordered ground state. Unlike the bipartite square lattice, the non-bipartite kagomé lattice is not topologically constrained, making our system more closely resemble the ice state studied in Ref. [22] than that considered in Ref. [23]. Although Fig. 4(c) shows that there is some tendency for the defected vertices to form pairs, there are no extended defect patterns of the type seen in Fig. 2. Since the ice rules in this system are enforced by the vortex-vortex interaction energies, we can weaken the enforcement of the ice rules by increasing the spacing a between pinning

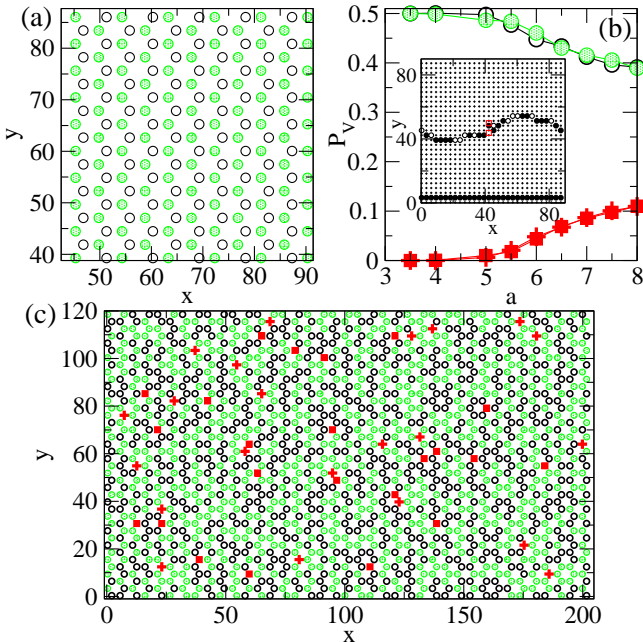


FIG. 4: (a) Ordered biased ground state in a sample with kagomé pinning, $f_b = 1.0$, $l = 2/3\lambda$, and $a = 3\lambda$. Open circles: $n_{in} = 1$ vertices; shaded circles: $n_{in} = 2$ vertices. (b) Percentage P_V of each vertex type vs a . Crosses: $n_{in} = 0$; open circles: $n_{in} = 1$; shaded circles: $n_{in} = 2$; filled squares: $n_{in} = 3$. Inset: grain boundary image in square ice sample with two doubly occupied pins (open squares) with the same symbols as in Fig. 2. (c) Vertex configuration after thermal annealing in a sample with $a = 3.5\lambda$, $l = 2/3$, and $f_b = 1.0$. Symbols are the same as in the main panel of (b).

sites. Figure 4(b) shows that as a increases, the system passes from a limit in which only kagomé-ice-rule obeying vortices appear for $a \leq 4\lambda$ to a limit $a \geq 8\lambda$ where the vertices assume a completely random arrangement.

In the random limit we expect to find each of the two defect vertex types with probability $1/8$ and each of the two kagomé-ice-rule obeying vertices with probability $3/8$.

There are other arrays that would obey ice-rule type constraints; however, the simplest cases for 2D are the square and kagomé arrays. Previous studies of superconducting wire networks arranged in kagomé configurations found geometrical frustration which produced disordered ground states [24]; however, such a system does not specifically have ice-rule obeying states. The artificial ice vortex system proposed here can be used to study the effect of ice-rule and non-ice-rule configurations on transport and magnetization properties, and it would also be possible to examine higher matching fields to see whether new types of ordered or disordered states appear.

In summary, we propose that square and kagomé vortex ice can be realized in nanostructured superconductors. By using an annealing protocol of a rotating externally applied current, the system can reach or approach the square ice ground state. In the presence of quenched disorder, defects appear in an ordered ground state background. For moderate disorder in the square ice system, all of the defects are bound to grain boundaries, while for strong disorder, individual high energy vertices proliferate. For kagomé ice, we find no grain boundary phase in the presence of disorder. We predict that if the barrier for vortex motion across the center of each artificial pinning site is weak, the system will spontaneously organize into a partially ordered state even without use of an annealing protocol. This system could have interesting transport and memory effects which may manifest themselves as changes in the critical current, an effect which cannot be accessed readily in other artificial ice systems.

We thank C. Nisoli for a useful discussion. This work was carried out under the NNSA of the U.S. DoE at LANL under Contract No. DE-AC52-06NA25396.

[1] L. Pauling, J. Am. Chem. Soc. **57**, 2680 (1935).
[2] P.W. Anderson, Phys. Rev. **102**, 1008 (1956).
[3] R. Moessner and A.P. Ramirez, Phys. Today, **59**(2), 24 (2006).
[4] A.P. Ramirez *et al.*, Nature (London) **399**, 333 (1999).
[5] Y. Han *et al.*, arXiv:0807.3905.
[6] H. Frauenfelder, P.G. Wolynes, and R.H. Austin, Rev. Mod. Phys. **71**, S419 (1999); H.M. Harreis, C.N. Likos, and H. Löwen, Biophys. J. **84**, 3607 (2003).
[7] C. Castelnovo, R. Moessner, and S.L. Sondhi, Nature **451**, 42 (2008); L.A.S. Mol *et al.*, arXiv:0809.2105.
[8] R.F. Wang *et al.*, Nature (London) **439**, 303 (2006).
[9] C. Nisoli *et al.*, Phys. Rev. Lett. **98**, 217203 (2007).
[10] X. Ke *et al.*, Phys. Rev. Lett. **101**, 037205 (2008).
[11] G. Möller and R. Moessner, Phys. Rev. Lett. **96**, 237202 (2006).
[12] M. Tanaka *et al.*, Phys. Rev. B **73**, 052411 (2006).
[13] Y. Qi, T. Brintlinger, and J. Cumings, Phys. Rev. B **77**, 094418 (2008).
[14] A. Libál, C. Reichhardt, and C.J. Olson Reichhardt, Phys. Rev. Lett. **97**, 228302 (2006).
[15] M. Baert *et al.*, Phys. Rev. Lett. **74**, 3269 (1995).
[16] J.I. Martín *et al.*, Phys. Rev. Lett. **83**, 1022 (1999).
[17] K. Harada *et al.*, Science **274**, 1167 (1996).
[18] S.B. Field *et al.*, Phys. Rev. Lett. **88**, 067003 (2002); A.N. Grigorenko *et al.*, *ibid.* **90**, 237001 (2003).
[19] G. Karapetrov *et al.*, Phys. Rev. Lett. **95**, 167002 (2005).
[20] G. Karapetrov *et al.*, Appl. Phys. Lett. **87**, 162515 (2005).
[21] I.V. Grigorieva *et al.*, Phys. Rev. Lett. **99**, 147003 (2007).
[22] A.S. Wills, R. Ballou, and C. Lacroix, Phys. Rev. B **66**, 144407 (2002).
[23] R. Moessner and S.L. Sondhi, Phys. Rev. B **68**, 064411 (2003); S.V. Isakov, R. Moessner, and S.L. Sondhi, Phys. Rev. Lett. **95**, 217201 (2005).
[24] M.S. Rzchowski, Phys. Rev. B **55**, 11745 (1997); D. Davidovic *et al.*, *ibid.* **55**, 6518 (1997); K. Park and D.A.

Huse, *ibid.* **64**, 134522 (2001); M.J. Higgins *et al.*, *ibid.* **61**, R894 (2000); Y. Xiao *et al.*, *ibid.* **65**, 214503 (2002).